

The Growth of Geological Structures by Repeated Earthquakes

2. Field Examples of Continental Dip-Slip Faults

ROSS S. STEIN

U.S. Geological Survey, Menlo Park, California

GEOFFREY C. P. KING

U.S. Geological Survey, Denver, Colorado

JOHN B. RUNDLE

Sandia National Laboratories, Albuquerque, New Mexico

A strong test of our understanding of the earthquake cycle is the ability to reproduce extant fault-bounded geological structures, such as basins and ranges, which are built by repeated cycles of deformation. Along strike-slip faults, the coseismic and interseismic deformation can be nearly equal in magnitude and opposite in sign, resulting in little permanent deformation except for the fault offset. For dip-slip faults, portions of the crust are lifted and dropped, and so buoyancy forces are exerted. The seismic and interseismic deformations do not balance, and structures grow and become subject to erosion and deposition. We consider three examples for which the structure and fault geometry are well known: the White Wolf reverse fault in California, site of the 1952 Kern County $M=7.3$ earthquake, the Lost River normal fault in Idaho, site of the 1983 Borah Peak $M=7.0$ earthquake, and the Cricket Mountain normal fault in Utah, site of Quaternary slip events. Basin stratigraphy and seismic reflection records are used to profile the structure, and coseismic deformation measured by leveling surveys is used to estimate the fault geometry. To reproduce these structures, we add the deformation associated with the earthquake cycle (the coseismic slip and postseismic relaxation) to the flexure caused by the observed sediment load, treating the crust as a thin elastic plate overlying a fluid substrate. The cumulative deformation is principally dependent on the elastic plate thickness, modestly sensitive to the sediment-substrate density difference, and insensitive to the fluid viscosity for the 4- to 8-Ma structures. We deduce a long-term flexural rigidity of 2.15×10^{19} Nm; this is equivalent to an elastic plate thickness of 2-4 km for a Young's modulus of 2.5×10^{10} Nm⁻². This value is found where independent estimates of the elastic thickness from the coherence between surface topography and gravity yield values of about 4 km, but where coseismic fault slip extends to a depth of 10-15 km. Thus much of the seismogenic crust must weaken substantially during the life of active faults, causing the fault-bounded basins to narrow over time.

INTRODUCTION

The process of earthquake strain accumulation and release provides direct information about how the Earth's crust deforms to create geological structures. In the companion paper [King *et al.*, this issue; hereafter Paper 1], we presented a kinematic model for the earthquake cycle that, for the first time, incorporates crustal flexure due to sediment loading and erosion. With this model we explored the spectrum of fault-bounded geological structures that could evolve for varying values of the elastic thickness of the crust and the amount of erosion and deposition. In this paper we examine three field examples of continental dip-slip faults. We reproduce these geological structures by using the coseismic deformation measured from leveling surveys to estimate the fault geometry, and the observed sediment load to determine the crustal flexure.

Our approach requires that the stratigraphy of both the

downthrown and upthrown fault blocks is known. Such examples are rare; typically basins are well preserved but ranges are eroded. Nonetheless, we focus on three structures where the upthrown fault block is either intact or can be reconstructed: the White Wolf fault bounding the San Joaquin Valley, California, site of the 1952 Kern County $M = 7.3$ thrust fault event; the Lost River fault bounding Thousand Springs Valley, site of the 1983 Borah Peak $M = 7.0$ normal fault shock; and the Cricket Mountain fault bounding Sevier Lake valley, Utah. The stratigraphy and evolution of these structures are estimated from oil well correlations, deep seismic-reflection profiles, geological maps, and gravity surveys. Although the stratigraphy of the Cricket Mountain fault is unusually clear, this fault has sustained no large historical earthquake, and so we assume a fault geometry typical of other basin and range events.

The strategy we use to reproduce these structures follows from two observations: (1) that earthquakes represent a significant contribution to the deformation of continental regions and (2) that similar earthquakes repeat on the same fault segments [e.g., Schwartz and Coppersmith, 1984]. For dip-slip faults, we envision that a repeating sequence of a large earthquake followed by slow

This paper is not subject to U.S. copyright. Published in 1988 by the American Geophysical Union.

Paper number 88JB03294

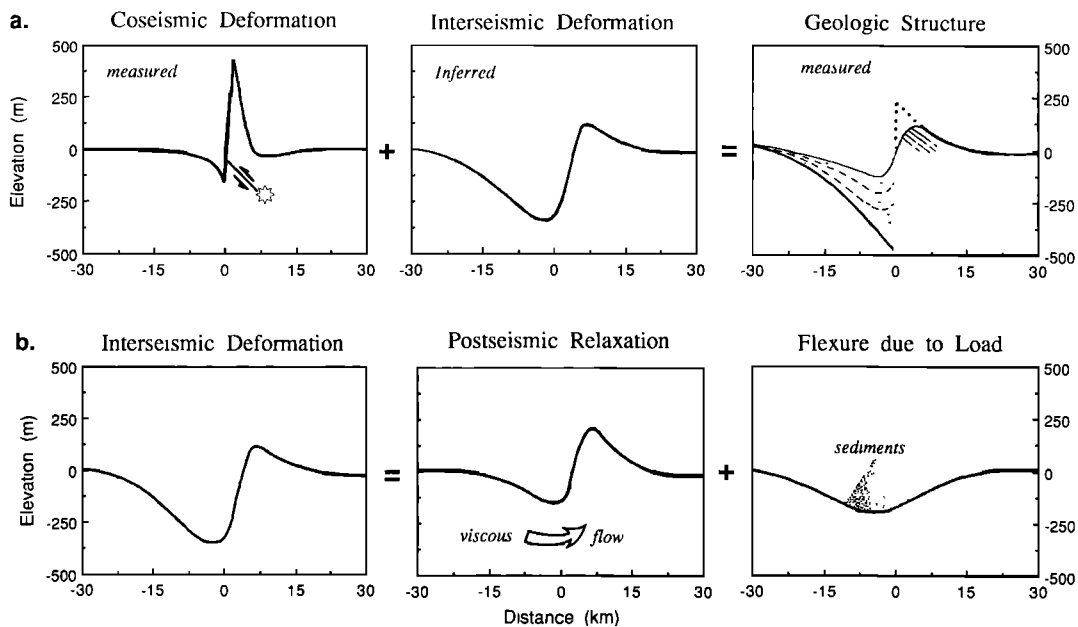


Fig. 1. (a) Schematic addition of sudden coseismic and slow interseismic deformation to generate the observed geological structure, modified by erosion (dotted) and deposition (stippled), for a 45°-dipping reverse fault with 1 km of cumulative slip. (b) Contributions of interseismic deformation shown in (Figure 1a). Arrow denotes viscous flow, and cone of sediment represents applied load (negative load due to erosion not shown). Coseismic deformation plus postseismic relaxation are referred to as the earthquake cycle in subsequent figures.

interseismic deformation creates the geological structure, as sketched in Figure 1a. If the coseismic and cumulative deformation for these structures are known, the unknown interseismic deformation can be deduced by subtracting the coseismic deformation from the cumulative deformation (the geological structure). The facsimile record of the earthquake cycle thus obtained is an average of thousands of events over the lifetime of the structure. We identify two principal contributions to the interseismic deformation and illustrate these in Figure 1b. Postseismic relaxation ensues because the viscous substrate flows to relieve stresses imposed by the earthquake and because buoyancy forces act to restore to isostatic equilibrium portions of the crust that were vertically displaced. Furthermore, crustal flexure occurs because the coseismic uplift of the range leads to erosion, and the subsidence leads to sediment transport and deposition into the basin.

FIELD SITES

White Wolf Fault, California

The White Wolf fault separates uplifted Mesozoic plutonic rocks of the southern Sierra Nevada batholith from a thick prism of Pliocene and Quaternary alluvium transported from the Sierra Nevada by the Kern River (Figure 2a). A cross section through the structure (Figure 3b) was constructed by Callaway [1969] from the logs of oil wells drilled to a maximum depth of 8.5 km; well locations are shown in Figure 2a. Extrapolating the upper Miocene Comanche sand on the upthrown block to the fault and correlating it with the contemporaneous Stenerup sand (both names of local usage) on the downthrown block yield a cumulative dip slip of 6-7 km. Because none of the

Miocene formations thickens toward the fault, most slip has occurred during the past 5-7 m.y. Structure contours drawn by Webb [1977] on an upper Miocene chert (Figure 2b) indicate a minimum of 5 km of vertical offset accompanied by 3-4 km of left-lateral slip.

The deformation associated with the 1952 Kern County $M = 7.3$ ($M_s = 7.7$) earthquake is shown in Figure 3a, measured along the leveling route shown in Figure 2a. Dunbar et al. [1980] and Stein and Thatcher [1981] modeled the coseismic elevation and horizontal strain changes to infer the earthquake faulting parameters. In the vicinity of the cross section, these studies suggest that about 2.5 m of dip slip and about 2 m of left-lateral slip occurred on a fault dipping 50°-70° and extending to a depth of 15-20 km.

The 1952 coseismic deformation differs from the Pliocene and Quaternary deformation in two respects (Figure 3). First, the earthquake deformation is wider, reckoned normal to the fault strike, than the deformation of the strata, particularly on the upthrown block. Second, the uplift of the upthrown side of the fault exceeds the subsidence of the downthrown side during the coseismic period, whereas the opposite is true for the Quaternary period. If the structure is the product of repeated cycles of coseismic and interseismic deformation, then the interseismic deformation must consist chiefly of downwarping centered over the fault, and a relaxation of deformation far from the fault.

Lost River Fault, Idaho

The Lost River fault is one of three adjacent 100-km-long normal faults active in central Idaho (Figure 4a). A geological map of the Thousand Springs Valley segment of the fault is shown in Figure 4b, and a schematic cross section normal to the fault in Figure 5b. Uplift of

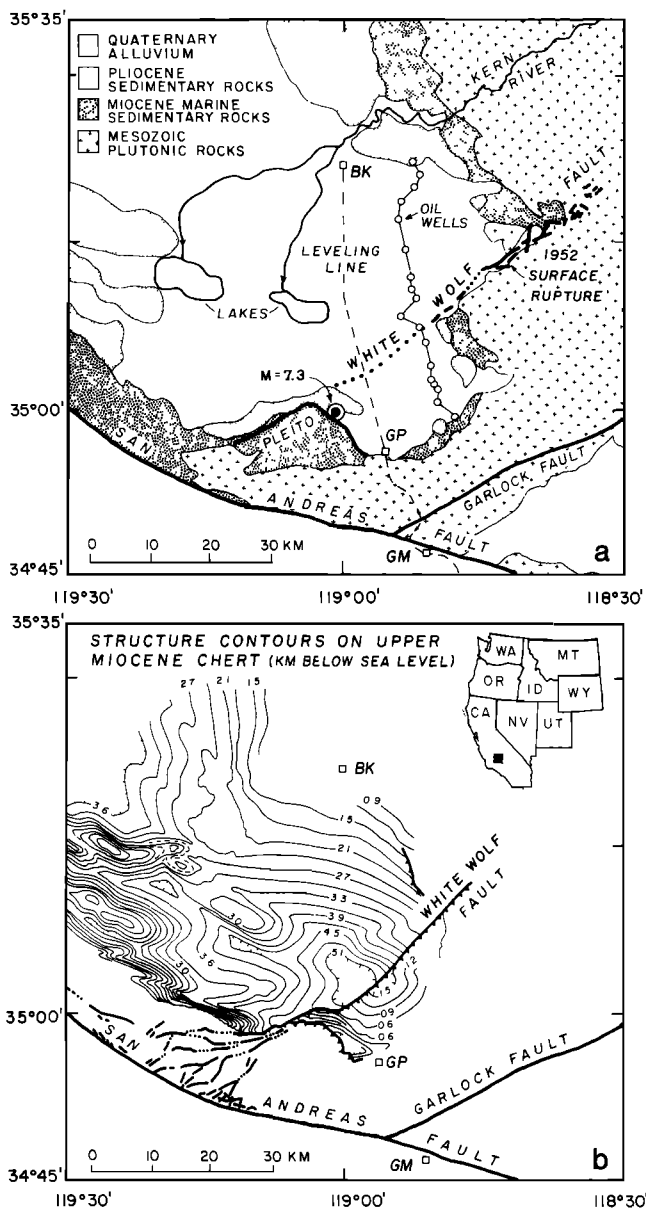


Fig. 2. (a) Geological map of the Kern County, California, area (simplified from Jennings [1977]), showing location of surface rupture and epicenter of the 1952 Kern County $M=7.3$ earthquake, leveling line (dashed) and wells used for stratigraphic cross section in Figure 2, and outlet of the Kern River before agricultural diversion, which drains the southern Sierra Nevada. BK, Bakersfield; GM, Gorman; GP, Grapevine. (b) Structure contours by Webb [1977] on an upper Miocene chert bed that has a characteristic signature on oil well electric logs in the Kern County area. Dotted line (inset) shows the location of the San Andreas fault.

Paleozoic rocks against the range-bounding normal faults has created the characteristic basin-and-range structure. The upthrown block, capped by Borah Peak, is better preserved and mapped here than anywhere else along the ranges. Scott *et al.* [1985] estimated that at least 3 km of dip slip has occurred along this segment of the Lost River fault during the past 4-7 m.y.

The 1983 Borah Peak $M=7.0$ ($M_S=7.3$) earthquake ruptured the Lost River fault for 30 km. A nearly identical event occurred along the same segment 6-8 ka [Hanks and

Schwartz, 1987]. Figure 5a shows a profile of the coseismic elevation changes measured along the leveling marked in Figure 4b. Stein and Barrientos [1985] and Barrientos *et al.* [1987] found that the geodetic data are best fitted by 2.0-2.2 m of normal slip extending from the surface to a depth of 13 ± 1 km on a fault dipping 45° - 50° . This result is also consistent with the seismic moment, fault plane solution, and depth (16 ± 4 km) of the October 28, 1983, main shock calculated by Doser and Smith [1985], as shown in Figure 5c.

The coseismic deformation extends for 15-20 km on each fault block (Figure 5a), similar to the width of the cumulative deformation. The coseismic subsidence, however, is 6 times greater than the coseismic uplift, whereas the cumulative uplift exceeds the cumulative subsidence. Thus interseismic deformation must consist of a broad upwarp, opposite to that inferred for the White Wolf fault.

Cricket Mountain Fault, Utah

The 30-km-long Cricket Mountain normal fault separates the Sevier Lake valley from uplifted Paleozoic sedimentary rocks of the Cricket Mountains (Figure 6). From the degree of degradation of the fault scarp in unconsolidated alluvium at the base of the range, Anderson and Bucknam [1979] estimated that this fault has been active during the past 0.5 m.y., although it has not produced a large surface rupture during the past 15 kyr. A seismic reflection profile (CGG 4), shown in Figure 7, crosses the north end of the fault where the upthrown block is buried and preserved from erosion (Figure 6), and thus presents an exceptionally clear stratigraphic record of both sides of the fault. A time section of the brightest reflectors at travel times less than 2 s is shown in Figure 8a. We converted this time section to a depth section, using the stacking velocities and depths of the original processing (Figure 8b) and also by reprocessing the record to reveal the deepest coherent reflectors (Figure 8c). Deformed strata extend for about 10 km from the fault trace on both sides of the fault, less far than at the Lost River fault. Beds above the dotted line in the middle panel of Figure 8b all converge or pinch out 8-10 km basinward of the fault trace, whereas those beds beneath the dotted line are concentrically folded. This structure indicates that the basin did not widen over time as it deepened and filled with sediment.

We require an estimate of the cumulative dip slip and the ratio of uplift to subsidence on the Cricket Mountain fault. The uplift and tilt of the upthrown fault block are recorded by reflections from a 4.2 ± 0.3 Ma basalt flow that crops out at the fault trace in the footwall [Lindsey *et al.*, 1980]. Because no published drilling records are available from Sevier Lake valley, it is unknown which basin reflector corresponds to this basalt flow. Von Tish *et al.* [1985] found that most high-angle normal faulting in the region occurred during the past 4 m.y., so we here assume that the fault became active largely after deposition of the basalt. This timing places the basalt in the position of the dotted line in Figure 8b. The net dip-slip displacement is then 4-5 km, and the cumulative ratio of uplift (1.5 km) to subsidence (2.2 km) is about 70%.

Lacking a record of coseismic deformation across the

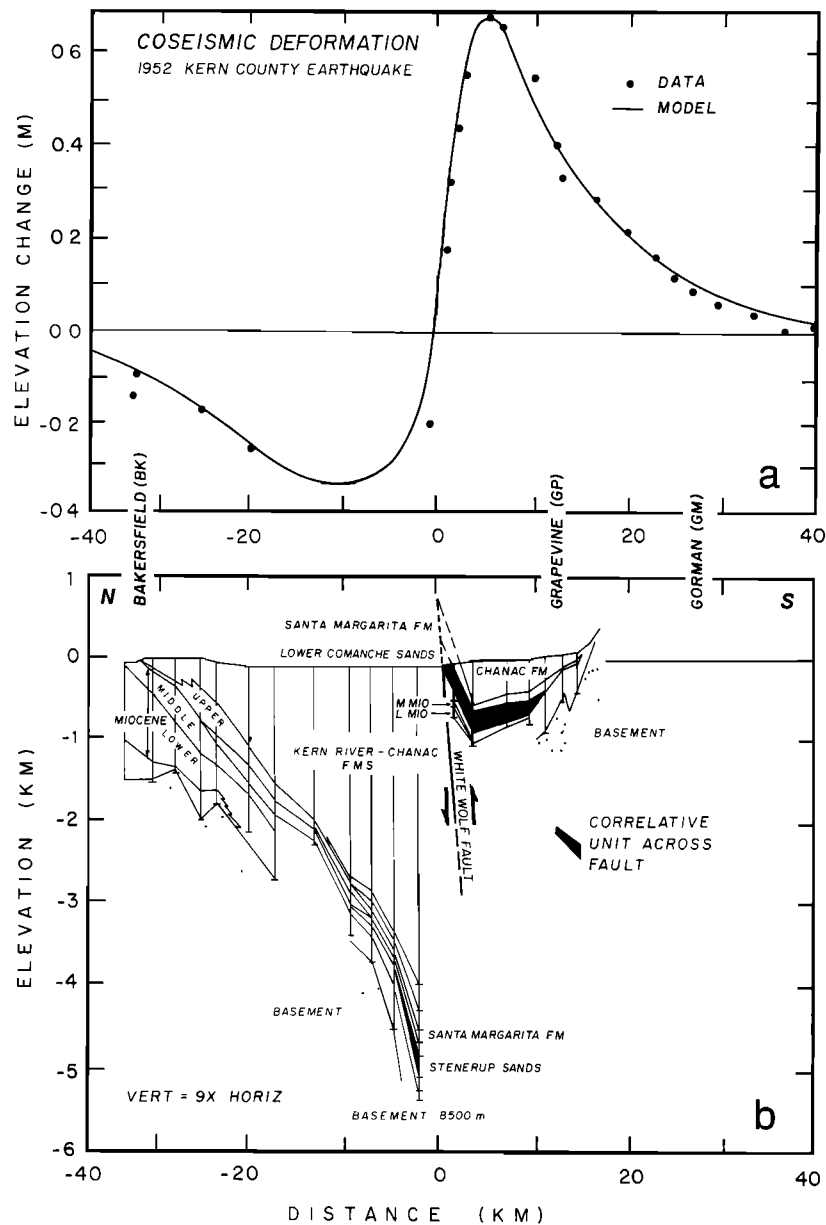


Fig. 3. (a) Coseismic deformation associated with the 1952 Kern County $M=7.3$ earthquake [from Stein and Thatcher, 1981]. (b) Kern River basin stratigraphy [from Callaway, 1969]. Contemporaneous units used to estimate the fault displacement are darkened. Routes for profiles are shown in Figure 2a.

Cricket Mountain fault, we assume that the fault dips 45° . The reflection record precludes a dip less than 40° in the upper 5 km (see Figures 8b and 8c). The seismic and geodetic evidence for all well-studied basin-and-range earthquakes yields dips of $45^\circ \pm 10^\circ$. (For the 1954 Fairview Peak-Dixie Valley earthquakes, see Savage and Hastie [1969], Snay et al. [1985], Okaya and Thompson [1985], and Doser [1986]. For the 1959 Hebgen Lake earthquake, see Savage and Hastie [1966], Doser [1985], and Barrientos et al. [1987]. For the 1983 Borah Peak earthquake, see Doser and Smith, [1985], and Stein and Barrientos, [1985].) If the 45° dip is a suitable choice for the Utah structure, then broad interseismic uplift must occur, similar to the pattern deduced for the Lost River fault. A discontinuous subhorizontal reflector at 8- to 10-km depth may be the Sevier desert detachment [Von Tish et al., 1985;

Allmendinger et al., 1986] seen on COCORP seismic reflection line UT1, located 20 km to the north (Figure 6).

MODELING STRATEGY AND ASSUMPTIONS

To limit the number of free parameters used to reproduce the structures, we do not explicitly treat the temporal decay of deformation after an earthquake but instead consider only the final relaxed form. Removal of time dependence from our analysis frees these results from reliance on knowledge of the loading history of the structures. The material beneath the elastic crust is treated as an inviscid fluid. We add the cumulative relaxed deformation (the summed earthquake cycles) and the cumulative crustal flexure caused by the sediment load. The net fault displacement and sediment load are approximately known, leaving the elastic

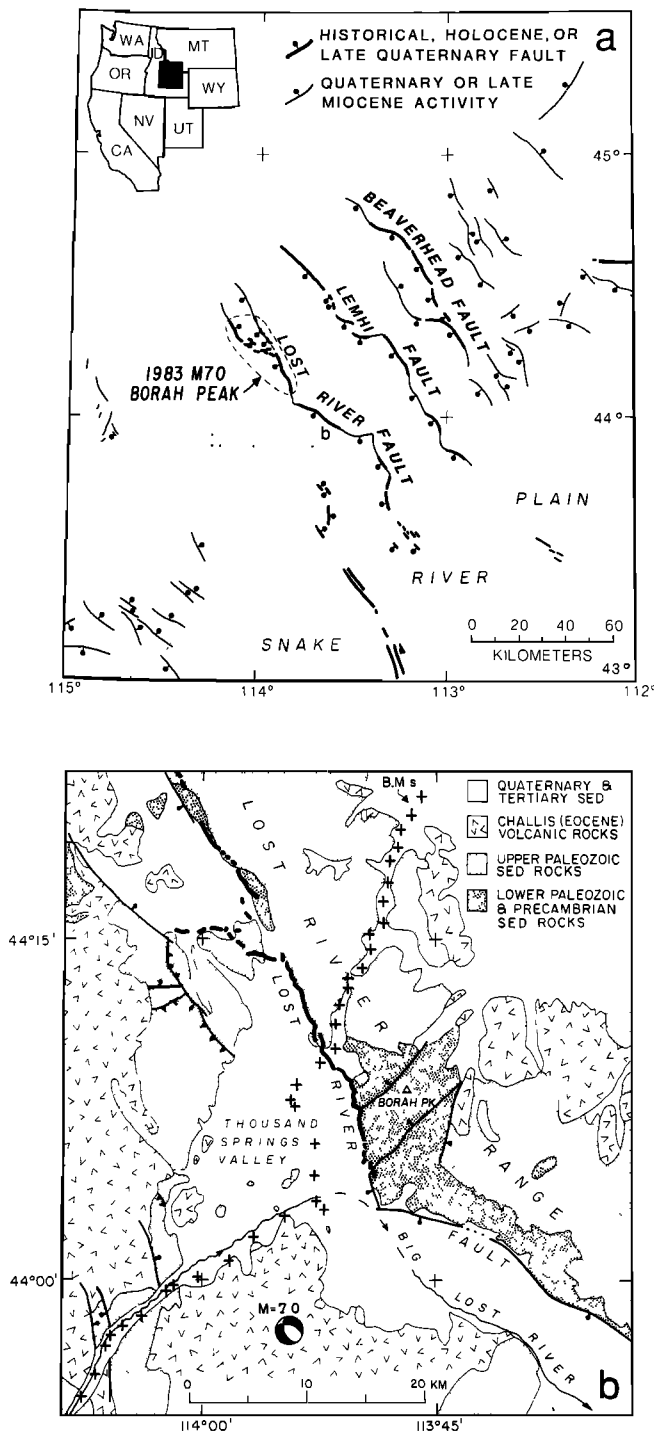


Fig. 4. (a) Northernmost basin and range province, Idaho. Dotted box denotes the location of Figure 4b. (b) Geological map of Thousand Springs valley segment of the Lost River fault, Idaho (simplified from Skipp and Harding, [1985]), showing locations of the Borah Peak $M=7.0$ earthquake, leveling bench marks (crosses), 1983 surface rupture (heavy lines), and course of the Big Lost River, which drains southward onto the Snake River Plain.

plate thickness, H , as the principal free parameter. The model is fully described in Paper 1, and the material properties assigned are listed in Table 1 of Paper 1. Key simplifications of the model are as follows.

Fault interactions. No interactions of adjacent faults are

considered, although the faults that we examined are not isolated features. Both the White Wolf and Lost River faults lie 30 km from major parallel faults and are closer to minor faults. Movement on adjacent faults alters the tilt of deformed beds, a process explored by Jackson and McKenzie [1983]. Depending on the fault spacing and dip direction, neglect of nearby faults could either increase or decrease the estimated elastic plate thickness. We have not tested multiple-fault models.

Horizontal displacements. We fit only the vertical component of displacements. The magnitudes of the horizontal and vertical displacements associated with a 45° -dipping fault are similar. Because the coseismic horizontal displacements are poorly known for these earthquakes and the long-term horizontal displacements are not well resolved in field structures, we cannot fit them directly. The fivefold to 10-fold vertical exaggeration in our figures reduces their significance in the model fitting.

Regional isostatic equilibrium. Postseismic relaxation and crustal flexure caused by mass movement are assumed to keep pace with earthquake deformation. The period required for structures to reach equilibrium is subject to dispute [see Cochran, 1980], and so it is uncertain whether the 4- to 8-m.y. time span that we consider is sufficient. An uncompensated load, such as recently deposited sediment, causes the elastic plate thickness to be underestimated unless the crust has a viscosity gradient (which increases with depth) rather than an elastic fluid interface, in which case the thickness would be overestimated.

Fault geometry. All faults are assumed to be planar and to dip 45° , the average inferred from the observed coseismic deformation. The relaxed deformation for an earthquake cycle is insensitive to modest ($\pm 15^\circ$) changes in dip, as we show in Figure 3 of Paper 1, and so we regard variable-dip modeling as unwarranted. We have not experimented with listric fault geometries (in which dip diminishes with depth). Listric faults would increase the asymmetry of the coseismic deformation, as investigated by Stein and Barrientos [1985], and perhaps reduce the magnitude of postseismic deformation if the fault does not cut through the elastic layer. Here, we comment only that listric-fault geometries are not required to satisfy either the coseismic or the long-term deformation.

Semi-infinite loads. The models we finally adopted use sediment loads that extend infinitely in the direction of the fault strike. Tests were performed with loads of limited extent, but once we saw that an elastic plate thickness in the range of 2-4 km (a tenth of the fault length) was needed, it was evident that two-dimensional loads were sufficient. The very thin elastic layer also means that large fault displacements are permissible without violating the model assumption of elasticity.

RESULTS

White Wolf Fault

The structure of the White Wolf fault, with the deep San Joaquin valley basin on the downthrown block and the small perched Grapevine Basin on the upthrown block, was

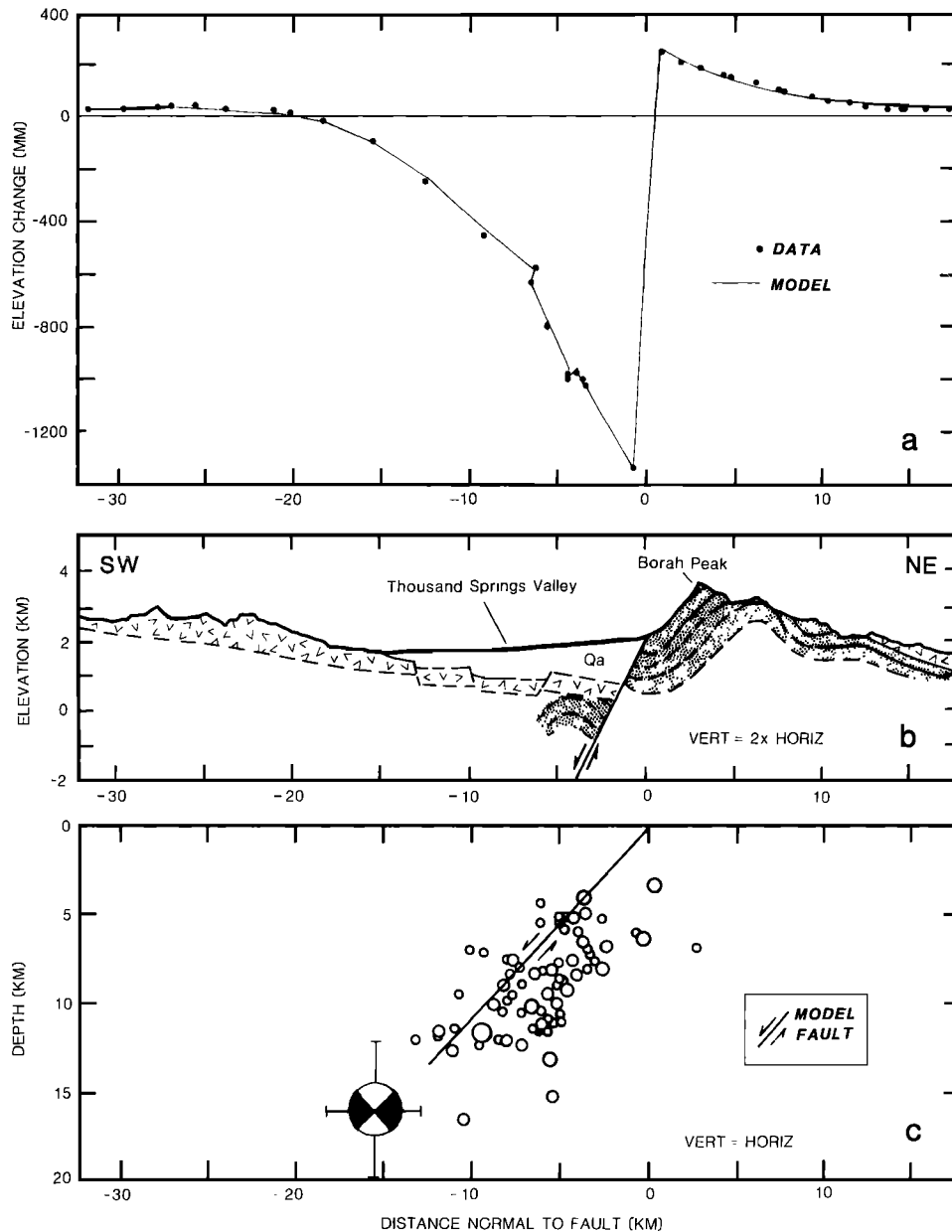


Fig. 5. (a) Coseismic deformation associated with the 1983 Borah Peak, Idaho, $M=7.0$ earthquake [from Stein and Barrientos, 1985] along route shown in Figure 4b, projected on an azimuth normal to the fault strike. (b) Geological cross section modified from Bond [1978] and Skipp and Harding [1985] using the gravity survey of Mabey [1985] and a seismic reflection profile of Smith et al. [1985]. Symbols as in Fig. 4b; Qa, Quaternary alluvial fill. (c) The 1983 aftershocks [from Richins et al., 1985] and mainshock [from Doser and Smith, 1985].

reproduced by using an elastic plate thickness, H , of 2 km. A greater plate thickness gives a deformation that is too broad, and a lesser plate thickness results in deformation that is too narrow and large. The upper Miocene marker horizon from Figure 2a and the estimated sediment load are plotted in Figure 9a. The columns extending downward are additions and those extending upward represent erosion from the upthrown block. The load is calculated by using 2.5-km-wide columns, assuming a sediment density, ρ_s , of $2.8 \times 10^3 \text{ kg m}^{-3}$ and the density of the fluid stratum underlying the crust, ρ_2 , of $3.0 \times 10^3 \text{ kg m}^{-3}$. The parameters are listed in Table 1. The flexure due to the sediment load is shown in Figure 9b. The White Wolf fault is taken to have a net dip slip of 6.75 km, on the basis of Figures 2 and 3b. We

refer to the sum of cumulative earthquake deformation and postearthquake relaxation as the earthquake cycle, as plotted in Figure 9b. The uplift for the earthquake cycle more nearly equals the subsidence than for the coseismic period (Figure 3a). The combined deformation of the earthquake, relaxation, and flexure is shown with the basin structure in Figure 9c.

Lost River Fault

Here deformation caused by the earthquake cycle dominates flexure due to loading. The net influx of sediment into the structure is small, and basin fill slightly exceeds range erosion (Figure 10a). Thousand Springs valley has been only been partly filled because the Big Lost

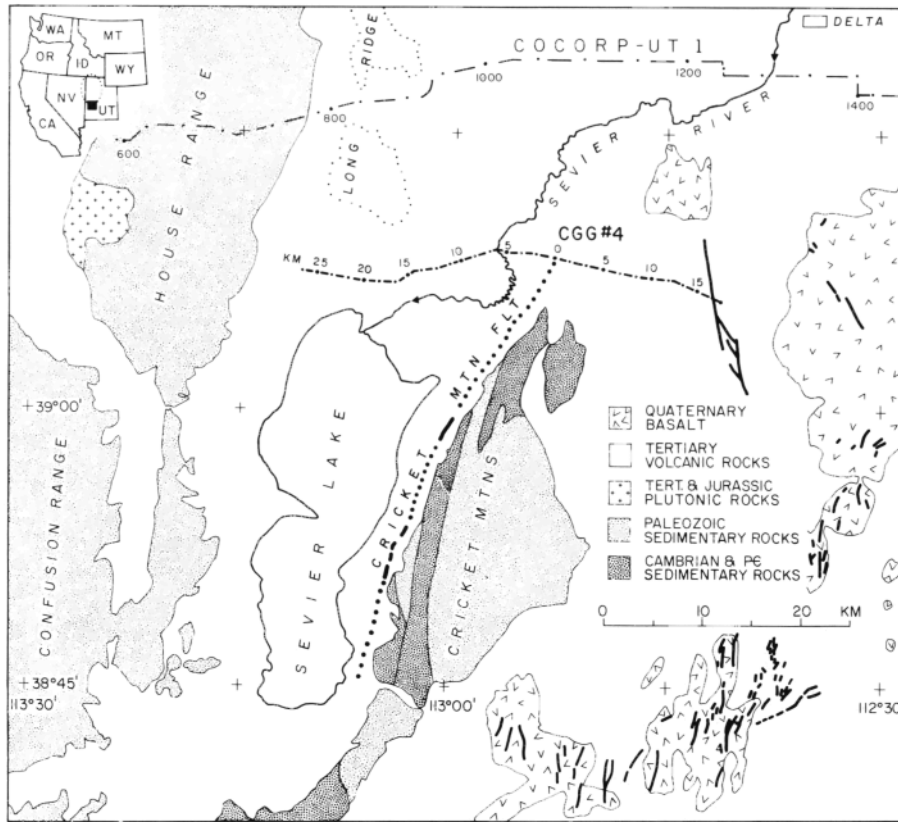


Fig. 6. Geological map of Cricket Mountain fault region, Utah, [from Von Tish et al., 1985], and faults active during the late Quaternary [from Anderson and Bucknam, 1979, Bucknam and Anderson, 1979], showing drainage into Sevier Lake, and locations of seismic-reflection profiles CCG 4, and COCORP-UT1 [from Allmendinger et al., 1986].

River drains into the Snake River Plain at lower elevation (Figure 4). The thin cover of sediments causes only a modest flexure, with maximum subsidence of about 200 m, and uplift of 70 m where the greatest load has been removed (Figure 10b). The Lost River fault was taken to have a cumulative dip slip of 4.25 km. The cumulative earthquake-cycle deformation is plotted in Figure 10b. Because of the normal sense of slip, the postseismic relaxation causes the region to uplift, unlike the White Wolf fault, and so the earthquake cycle yields nearly equal uplift and subsidence. The combined earthquake and flexural deformation, and the basin profile, is plotted in Figure 10c. The fit is imperfect, but so, too, is our knowledge of the geological structure. The ratio of uplift

to subsidence and the width of the total deformation agree best with the geological structure for an elastic plate thickness of 4 km, which is about a third of the coseismic faulting depth. The fit is insensitive to sediment density because so little fill is present. The fault parameters are listed in Table 1.

Cricket Mountain Fault

Sevier Lake forms a closed depression in the downthrown block of the Cricket Mountain fault, capturing much of the sediment eroded from the adjacent ranges. Thus the net influx of sediment lies between the larger load for the White Wolf and the smaller load for the Lost River

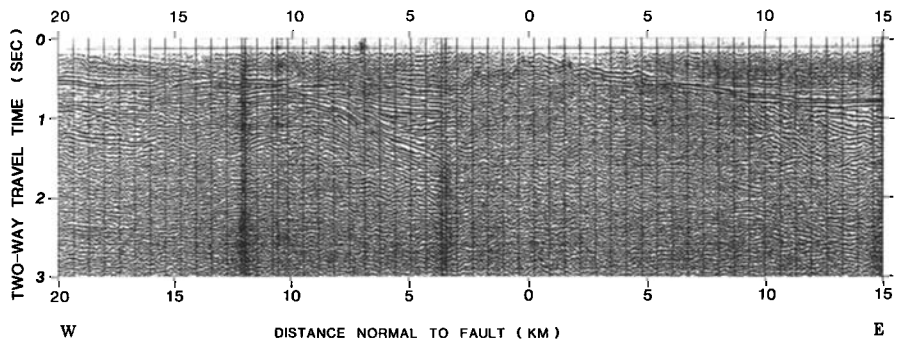


Fig. 7. Unmigrated seismic reflection profile CCG 4 across north end of the Cricket Mountain fault, purchased by U.S. Geological Survey from Consolidated Georex Geophysics.

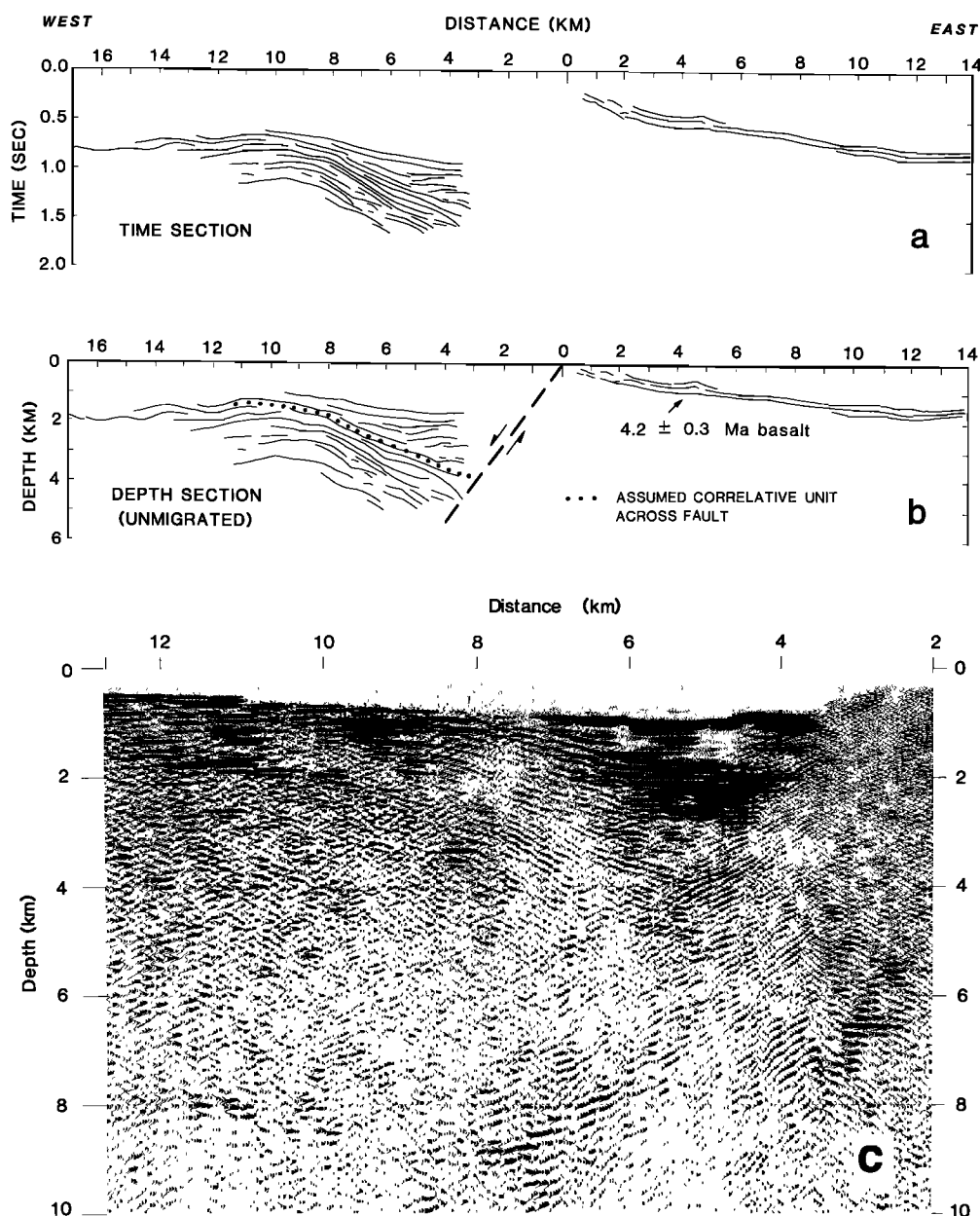


Fig. 8. Time section of brightest reflectors recorded at less than 2 s on the Cricket Mountain profile (a), converted to a depth section (b). Dotted line, probable position of basalt in the basin; strata below dotted line predate faulting. The complete time section was also converted to a depth section to reveal deeper reflectors (c).

fault (Figure 11a). Sediment deposition causes a maximum subsidence of about 400 m (Figure 11b). The Cricket Mountain fault is taken to have a cumulative dip slip of 6.5 km on an extent of 40 km along strike (see Table 1). The sum of the earthquake cycle and flexure for an elastic plate thickness of 2 km is plotted in Figure 11c. The ratio of uplift (1.5 km) to subsidence (3 km), and the breadth of the deformation accord well with the stratigraphy. The principal influence of the flexure is to broaden the deformation.

The effect of halving or doubling the elastic plate thickness is shown for the Cricket Mountain fault in Figure 12. The cumulative deformation for a plate thickness of 4 km is wider than the Cricket Mountain structure. The predicted deformation for a plate thickness of

1 km reproduces the observed profile for the downthrown block but is too narrow on the upthrown block. This pattern underscores the need to observe both the hanging wall and footwall blocks of the structure and suggests that, apart from any systematic error, our precision in estimating the elastic plate thickness is about ± 1 km.

DISCUSSION

Elastic Plate Thickness and Flexural Rigidity

These field examples suggest that earthquake deformation, postearthquake relaxation, and sediment loading are sufficient to account for the growth of geological structures bounded by active dip-slip faults. The

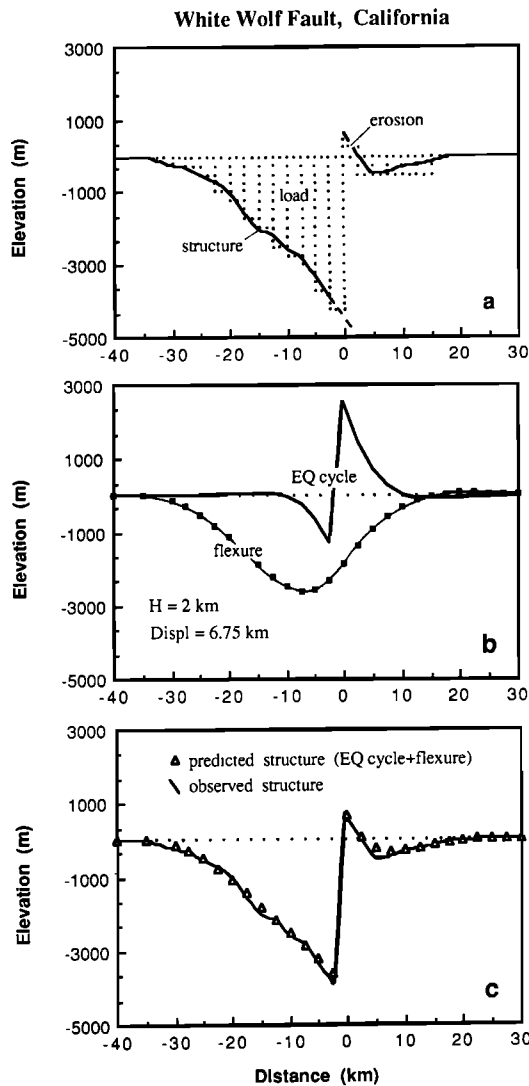


Fig. 9. Model fitted to the White Wolf fault. (a) Sediment load measured from observed basin structure. (b) Resulting flexure from loading, and cumulative earthquake cycle (coseismic deformation plus postseismic relaxation) after 6.75 km of net slip on the fault, for an elastic thickness of 2 km. (c) Predicted structure (earthquake cycle plus flexure due to loading) compared with observed structure from (Figure 9a).

data are fitted best when the elastic plate thickness is set to 2-4 km, which corresponds to a flexural rigidity of 10^{19} - 10^{20} Nm. The elastic plate thickness is about 1/4 the depth of coseismic fault slippage for the 1952 Kern County and 1983 Borah Peak earthquakes. We interpret this result to indicate that, at least near these active faults, portions of the crust relax imposed stresses. Various mechanisms are possible, including a loss of rigidity over a particular depth range or throughout isolated patches of the seismogenic crust.

The crustal flexure due to sediment load was modeled as a thin unfractured elastic plate overlying a fluid half-space. If, instead, the fault behaves as a weak zone that sustains interseismic slip and locally does not transmit torque, the wavelength of the flexure could be reduced to three-fourths of the value we deduce, and the amplitude of the flexure could be twice our value [McNutt, 1980, Fig. 3; Turcotte and Schubert, 1982, p. 127]. As we show in Paper 1, the

elastic thickness is almost inversely proportional to the flexural wavelength, and so we may be underestimating the elastic thickness by as much as 50%. To obtain the correct flexural amplitude, however, would require a sediment load of about half our assigned values, which seems prohibitively small. Alternative realizations of a weak crust encompass a thick crust with a plastic yield strength, as modeled for mid-oceanic rifts by Lin and Parmentier [1988], or a thick, pervasively fractured crust. If the viscous material were confined to a subcrustal layer with a thickness as little as several kilometers, and if relaxation of stresses is incomplete, then we could have underestimated the elastic thickness by 1-2 km, as we illustrate in Figure 11 of Paper 1. Incomplete stress relief is possible only if the earthquake repeat time is small relative to the characteristic relaxation time of the fluid.

We can invoke some independent support for our deduction of a weak crust. Investigations of the coherence between surface topography and Bouguer gravity by Forsyth [1985] Bechtel and Forsyth [1987], and Bechtel et al. [1987] yield elastic plate thickness estimates of about 3-5 km for the sites we investigated. Because the basin-

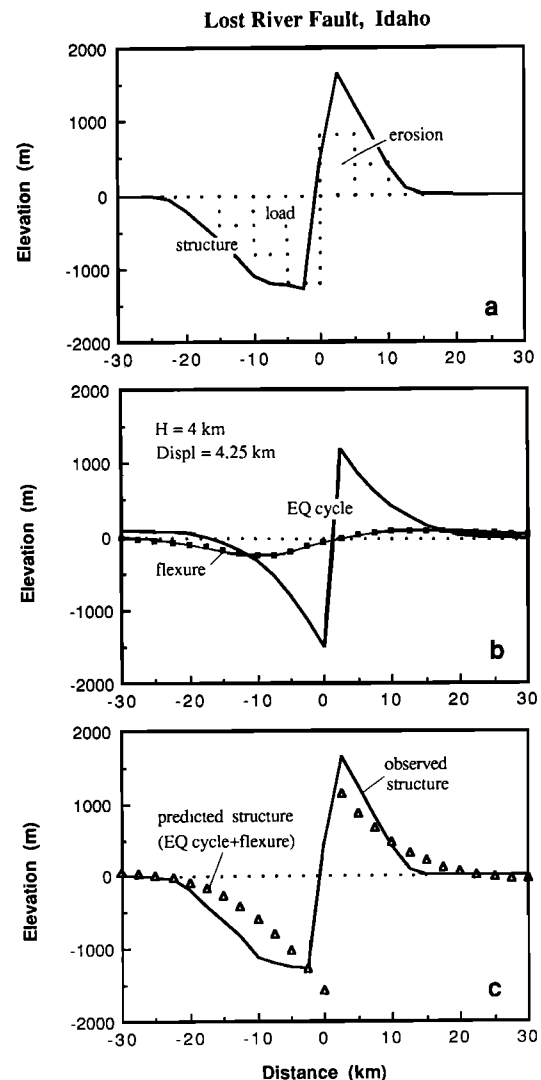


Fig. 10. Model fitted to the Lost River fault. (Same symbols as in Figure 9).

TABLE 1. Fault Parameters

Fault	Age, Ma	Cumulative Displacement, km	Modeled				Deduced*	
			Fault Dip, deg	Fault Length, km	Sediment Density, 10^3 kg m^{-3}	Lower Crust-Sediment Density Difference, 10^3 kg m^{-3}	Elastic Thickness, km	Flexural Rigidity, Nm
White Wolf, California	5-7	6.75 reverse	45	40	2.8	0.2	2	2.0×10^{19}
Lost River, Idaho	4-7	4.25 normal	45	80	2.7	0.8	4	1.5×10^{20}
Cricket Mtn., Utah	5-8	6.50 normal	45	40	2.7	0.8	2	2.0×10^{19}

*Assuming that E , Young's modulus, is $2.5 \times 10^{10} \text{ Nm}^{-2}$, and ν , Poisson's ratio, is 0.25.

and-range topography corresponds closely to the geological structure, the age and scale of the structures subject to coherence analysis are similar to ours and thus should yield similar results. In contrast, studies of the postglacial rebound of Lake Bonneville, Utah, suggest an elastic plate thickness of about 20-25 km [Nakiboglu and Lambeck, 1983; Bills and May, 1987]. The Cricket Mountain fault lies at the south margin of Lake Bonneville (see inset, Figure 6), so although the Bonneville load is 10 times wider (400 km by 300 km) than the structures we examined, our results should coincide. It is possible that the Bonneville load responds principally to the mantle relaxation, whereas the smaller fault-bounded structures are relaxed by a shallower but thinner viscoelastic layer in the lower crust. The Lake Bonneville load has little power at the short wavelengths (30 km) that we examine. Consequently the postglacial rebound is not sensitive to the effects we consider.

Our finding of an effective elastic plate thickness less than the depth of coseismic faulting may resolve an outstanding ambiguity about the mechanical behavior of the San Andreas fault. Thatcher [1983] showed that the geodetic data for a single composite earthquake cycle on the San Andreas fault cannot be used to distinguish between a thin or thick elastic crust. In the thin crust model, earthquake slip extends from the ground surface to the base of the elastic crust, and interseismic deformation results from flow in the subcrustal material caused by stress relaxation, similar to our model. In the thick-crust model, transient motions are caused by postearthquake aseismic slip on a fault that continues beneath the coseismic slip plane within the elastic crust. For dip-slip earthquakes, however, the addition of crustal flexure caused by the sediment load allows a sharp distinction to be drawn between these extremes: Our data are incompatible with a thick crust. Because the White Wolf fault lies only 15 km from the San Andreas fault (Figure 2), the thin crust model favored for dip-slip faults may be equally applicable to the San Andreas fault.

Sediment Supply and Interseismic Deformation

The coseismic surface depression changes shape as the postseismic relaxation proceeds. This process and the

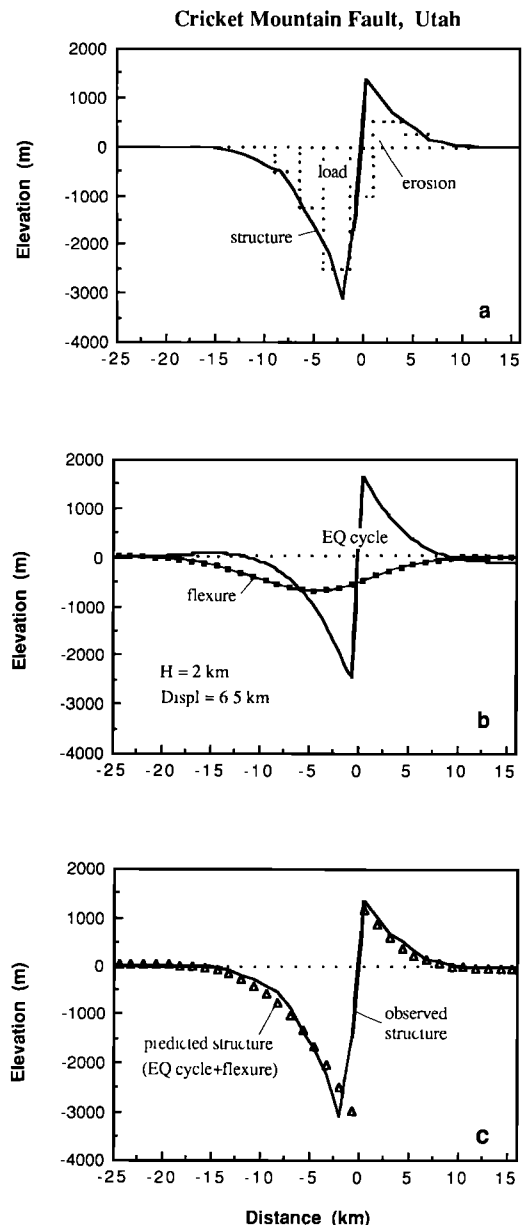


Fig. 11. Model fitted to the Cricket Mountain fault. (Same symbols as in Figure 9).

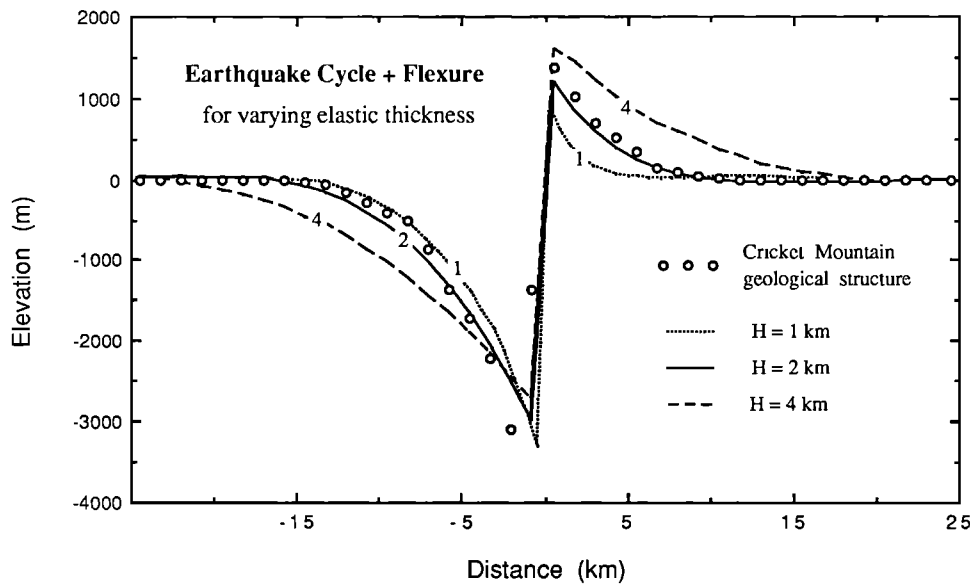


Fig. 12. Model fitted to the Cricket Mountain fault structure for three values of elastic plate thickness, H . The sediment load and net displacement are the same as in Figure 11.

supply of sediment control the eventual shape of the geological structure. After large normal faulting earthquakes, the basin shallows and the range is uplifted, whereas after reverse-faulting events, the basin deepens and the range subsides. Unless sediment fills the basin rapidly after an earthquake (early in the earthquake cycle), a normal-faulting structure will slowly uplift and erode the range. Thousand Springs valley is such a partly filled basin, with Borah Peak rising 1.5 km above the fault trace. In contrast, the sediment supply into Sevier Lake valley was great enough to fill the basin and bury the north end of the upthrown block of the Cricket Mountain fault. The southern San Joaquin valley bounding the White Wolf thrust fault has a nearly inexhaustible sediment supply, leading to downwarping of the structure due to the sediment load, and scant erosion of the upthrown block. Thus whereas the postseismic transient deformation depends exclusively on the fault geometry, the final form of the structure also depends on the sediment supply, as illustrated in Paper 1 (Figures 8 and 9).

Both earthquake and postearthquake deformation may be periodic over time, but the flexure due to sediment loading may, instead, be steady or episodic. Examples of rivers flooding fault-bounded basins and depositing sediment hours after a large earthquake include the 1980 El Asnam, Algeria shock reported by *King and Vita-Finzi* [1981], the 1983 Borah Peak earthquake [*Whitehead et al.*, 1984], and the 1959 Hebgen Lake earthquake [*Hadley*, 1964]. In these events, the coseismic deformation and emplacement of the load may nearly coincide. Other geological structures are known for which climatic or tectonic changes altered the drainage patterns or sediment supply. The ancestral Kern River drained westward to the Pacific Ocean until uplift of the California Coast Ranges blocked its outlet to the sea 5-2 Ma [*Page and Engebretson*, 1984], whereupon the downthrown block of the White Wolf fault began to fill rapidly. The presence of extensive outwash-fan deposits dated approximately at 12-14 kyr along much of the Lost River fault [*Scott et al.*, 1985; *Hanks and Schwartz*, 1987]

suggests that climatic changes have controlled the timing of sediment emplacement into many basin and range structures.

Application to Underthrust Zones

Flexure due to sediment loading may be an important addition to models of the earthquake cycle and long-term deformation along underthrust zones. Submarine trenches adjacent to the Pacific Northwest coast of the United States, Alaska, and Japan are subject to great erosion and sediment transport from the coastal landmass, whereas those adjacent to largely submerged volcanic arcs, such as the Aleutian or Kurile islands, receive only pelagic (seafloor) sediment scraped off the subducting oceanic plate. *Sato and Matsu'ura* [1988] successfully matched the observed bathymetry and free-air gravity profiles across the Kurile Trench in northern Japan using a viscoelastic dislocation model. Neglect of sediment deposition by these authors resulted in a misfit to the depth of the subducting oceanic plate, which is depressed as a result of pelagic sediment accumulation. Back arc basins, such as the Japan Sea, also fill with sediment and downwarp. In general, the long-term uplift will be overestimated if sediment loading is neglected.

Thatcher [1984] synthesized a complete earthquake cycle at a convergent plate margin at the Nankai Trough, Japan. He compared the cumulative, geodetically measured deformation for the 90-year-long cycle with the uplift on the marine terrace at the same locality, 140-180 km landward of the trench. Although the movement patterns of the 90-year-long cycle and the 120-kyr terrace are similar, the rates are not: the rate of terrace uplift is only 30% of the geodetically measured rate. The explanation for this discrepancy may lie in the downward flexure of the shoreline caused by rapid deposition of sediment into the trench and inland sea. This explanation could be verified by examining the plate flexure caused by the past 120 kyr of sediment deposition.

CONCLUSIONS

We have argued in this and the companion Paper 1 that two interacting processes govern the evolution of fault-bounded geological structures: the earthquake cycle of strain accumulation and release, and the flexure of the crust due to sediment deposition and erosion. We have sought to reproduce the cumulative deformation for three continental dip-slip faults by adding the coseismic deformation due to sudden fault slip, the postseismic relaxation due to buoyant and viscous restoring forces, and the flexure due to sediment loading. Our models, however, are not unique: although we have explained the observations for two out of the three structures studied, we have not necessarily explained them correctly. What we have done is to address the evolution of large structures on the basis of what we observe to occur on the same scale at present.

The similar width of the observed coseismic and cumulative deformation for the White Wolf and Lost River faults supplies the principal constraint for this work. This requirement leads to a paradox because the viscous and buoyant restoring forces act at greater depth than the coseismic deformation and thus cause a surface deformation wider than the coseismic deformation. In addition, the crustal flexure caused by basin infilling must be wider than the basin into which the sediment is deposited, and the flexural wavelength increases with the elastic plate thickness.

This paradox can be resolved, however, if the crust weakens over time after each earthquake or, stated differently, if the effective plate thickness of the crust over several million years averages about 2-4 km (at most, 3-6 km), i.e., 20-40% of the thickness over which earthquake faulting occurs.

Independent support for our deduction of a weak crust comes from the coherence between surface topography and Bouguer gravity for the western United States. This work suggests an elastic plate thickness of 3-8 km if large lower-crustal density variations are present [Forsyth, 1985; Bechtel and Forsyth, 1987]. Even the larger value is about half the maximum depth of earthquakes in the regions we consider, the Basin and Range and the California Coast Ranges. Thus these coherence investigations share our requirement that the crust must have sufficient long-term strength to rupture in large earthquakes, but yield appreciably between earthquakes. Studies of the much younger and broader Lake Bonneville rebound [Bills and May, 1987] provide estimates of the elastic-plate thickness, 20-25 km, about twice the depth of seismic faulting—in conflict with our results.

An ancillary conclusion of our study is that the interaction between postseismic relaxation and flexure leads to different evolutionary paths for normal and reverse fault structures. Whereas a normal fault basin is largest immediately after an earthquake and becomes shallower throughout the interseismic period, a basin bounded by an active reverse fault deepens during the cycle and thus may be more effective at capturing and holding sediment. Therefore the way in which sedimentary loading and erosional unloading occur before the earthquake-induced stresses have fully relaxed is the origin of the differences between fault-bounded geological structures. Consideration

of crustal flexure caused by sediment loading may also be a promising avenue of research for the study of underthrust zones.

Acknowledgments. We thank Wayne Thatcher for his insight and encouragement of our work. We are grateful to Jill McCarthy for reprocessing seismic reflection profile CGG 4. Jian Lin, James Savage, David Schwartz, Maria Zuber, and an anonymous referee contributed thoughtful reviews of the manuscript.

REFERENCES

- Allmendinger, R. W., H. Farmer, E. Hauser, J. Sharp, D. Von Tish, J. Oliver, and S. Kaufman, Phanerozoic tectonics of the Basin and Range--Colorado Plateau transition from COCORP data and geologic data: A review, *Reflection Seismology: The Continental Crust, Geody. Ser. Edited by M. Barrangi and L. Brown, p.p. 14, 257-267*, AGU, Washington, D.C., 1986.
- Anderson, R. E., and R. C. Bucknam, Map of fault scarps in unconsolidated sediments, Richfield 1° by 2° quadrangle, Utah, *U.S. Geol. Surv. Open - File Rep.*, 79-1236, 1979.
- Barrientos, S. E., R. S. Stein, and S. N. Ward, Comparison of the 1959 Hebgen Lake, Montana and the 1983 Borah Peak, Idaho, earthquakes from geodetic observations, *Bull. Seismol. Soc. Am.*, 77, 784-808, 1987.
- Bechtel, T. D., and D. W. Forsyth, Isostatic compensation in the Basin and Range, U.S.A., *Eos Trans. AGU*, 68, 1450, 1987a.
- Bechtel, T. D., D. W. Forsyth, and M. T. Zuber, Variations in effective elastic thickness of continental lithosphere, *Int. Un. Geod. Geophys., XIX Gen. Assem., Abstracts*, 1, 300, 1987. (*Vancouver, Canada*)
- Bills, B. G., and G. L. May, Lake Bonneville: Constraints on lithospheric thickness and upper mantle viscosity from isostatic warping of Bonneville, Provo and Gilbert stage shorelines, *J. Geophys. Res.*, 92, 11,493-11,508, 1987.
- Bond, J. G., Geologic map of Idaho, Idaho Bur. Mines Geol., Moscow, 1978.
- Bucknam, R. C., and R. E. Anderson, Map of fault scarps on unconsolidated sediments, Delta 1° by 2° quadrangle, Utah, *U.S. Geol. Surv. Open - File Rep.*, 79-366, 1979.
- Callaway, D. C., Correlation Section 17, San Joaquin Valley: Kingsburg to Tejon Hills, Pacific Section, Am. Assoc. Petrol. Geol., Tulsa, Okla., 1969.
- Cochran, J. R., Some remarks on isostasy and the long term behavior of continental lithosphere, *Earth Planet. Sci. Lett.*, 46, 266-274, 1980.
- Doser, D. I., Source parameters and faulting processes of the 1959 Hebgen Lake, Montana, earthquake sequence, *J. Geophys. Res.*, 90, 4537-4556, 1985.
- Doser, D. I., Earthquake processes in the Rainbow Mountain-Dixie Valley, Nevada, region 1954-1959, *J. Geophys. Res.*, 91, 572-586, 1986.
- Doser, D. I., and R. B. Smith, Source parameters of the 28 October 1983 Borah Peak, Idaho, earthquake from body wave analysis, *Bull. Seismol. Soc. Am.*, 75, 1041-1051, 1985.
- Dunbar, W. S., D. M. Boore, and W. Thatcher, Pre-, co-, and post-seismic strain changes associated with the 1952 $M_L=7.2$ Kern County, California, earthquake, *Bull. Seismol. Soc. Am.*, 70, 1893-1905, 1980.
- Forsyth, D. W., Subsurface loading and estimates of the flexural rigidity of continental lithosphere, *J. Geophys. Res.*, 90, 12,623-12,632, 1985.
- Hadley, J. B., Landslides and related phenomena accompanying the Hebgen Lake earthquake of August 17, 1959, *U.S. Geol. Surv. Prof. Pap.*, 435-K, 107-138, 1964.
- Hanks, T. C., and D. P. Schwartz, Morphologic dating of the pre-1983 fault scarp on the Lost River fault at Doublesprings Pass Road, Custer County, Idaho, *Bull. Seismol. Soc. Am.*, 77, 837-846, 1987.

- Jackson, J., and D. McKenzie, The geometrical evolution of normal fault systems, *J. Struct. Geol.*, 5, 471-482, 1983.
- Jennings, C. W., Geologic map of California, Calif. Div. Mines and Geol., Sacramento, 1977.
- King, G. C. P., and C. Vita-Finzi, Active folding in the Algerian earthquake of 10 October 1980, *Nature*, 292, 22-26, 1981.
- King, G.C.P., R.S. Stein, J.B. Rundle, The growth of geological structures by repeated earthquakes: 1, Conceptual framework, *J. Geophys. Res.*, this issue.
- Lin, J., and M. Parmentier, Mechanics of lithospheric extension at mid-ocean ridges. *Geophys. J. R. Astron. Soc.*, 91, in press, 1988.
- Lindsey, D. A., R. K. Glanzman, C. W. Naiser, and D. J. Nichols, Upper Oligocene evaporites in basin fill of Sevier Desert region, western Utah, *Am. Assoc. Petrol. Geol. Bull.*, 62, 251-260, 1980.
- Mabey, D. R., Regional gravity and magnetic anomalies in the Borah Peak region of Idaho, *U.S. Geol. Surv. Open-File Rep.*, 85-290, 680-686, 1985.
- McNutt, M., Implications of regional gravity for state of stress in the Earth's crust and upper mantle, *J. Geophys. Res.*, 85, 6377-6396, 1980.
- Nakiboglu, S. M., and K. Lambeck, A reevaluation of isostatic rebound of Lake Bonneville, *J. Geophys. Res.*, 88, 10,439-10,447, 1983.
- Okaya, D. A., and G. A. Thompson, Geometry of Cenozoic extensional faulting: Dixie Valley, Nevada, *Tectonics*, 4, 107-126, 1985.
- Page, B. M., and D. C. Engebretson, Correlation between the geologic record and computed plate motions for central California, *Tectonics*, 3, 133-156, 1984.
- Richins, W. D., R. B. Smith, C. J. Langer, J. E. Zollweg, J. T. King, and J. C. Pechmann, The 1983 Borah Peak, Idaho, earthquake: Relationship of aftershocks to the mainshock, surface faulting, and regional tectonics, *U.S. Geol. Surv. Open - File Rep.*, 85-290, 285-310, 1985.
- Sato, T., and M. Matsu'ura, A kinematic model for the deformation of the lithosphere at subduction zones, *J. Geophys. Res.*, 93, 6410-6418, 1988.
- Savage, J. C., and L. M. Hastie, Surface deformation associated with dip-slip faulting, *J. Geophys. Res.*, 71, 4897-4904, 1966.
- Savage, J. C., and L. M. Hastie, A dislocation model for the Fairview Peak, Nevada, earthquake, *Bull. Seismol. Soc. Am.*, 59, 1937-1948, 1969.
- Schwartz, D. P., and K. J. Coppersmith, Fault behavior and characteristic earthquakes: Examples from the Wasatch and San Andreas fault zones, *J. Geophys. Res.*, 89, 5681-5698, 1984.
- Scott, W. E., K. L. Pierce, and M. H. Hait, Jr., Quaternary tectonic setting of the 1983 Borah Peak earthquake, Central Idaho, *Bull. Seismol. Soc. Am.*, 75, 1053-1066, 1985.
- Skipp, B., and S. T. Harding, Preliminary report on geology of Borah Peak area, Idaho, including interpretation of seismic and gravity data, *U.S. Geol. Surv. Open-File Rep.*, 85-290, 657-671, 1985.
- Smith, R. B., W. D. Richins, and D. I. Doser, The 1983 Borah Peak, Idaho, earthquake: Regional seismicity, kinematics of faulting, and tectonic mechanism, *U.S. Geol. Surv. Open-File Rep.*, 85-290, 236-263, 1985.
- Snay, R. A., M. W. Cline, and E. L. Timmerman, Dislocation model for the 1954 Nevada earthquakes, *U.S. Geol. Surv. Open-File Rep.*, 85-290, 531-555, 1985.
- Stein, R. S., and S. E. Barrientos, Planar high-angle faulting in the Basin and Range: Geodetic analysis of the 1983 Borah Peak, Idaho, earthquake, *J. Geophys. Res.*, 90, 11,355-11,366, 1985.
- Stein, R. S., and W. Thatcher, Seismic and aseismic deformation associated with the 1952 Kern County, California, earthquake and relationship to the Quaternary history of the White Wolf fault, *J. Geophys. Res.*, 86, 4913-4928, 1981.
- Thatcher, W., Nonlinear buildup and the earthquake cycle on the San Andreas fault, *J. Geophys. Res.*, 88, 5893-5902, 1983.
- Thatcher, W., The earthquake deformation cycle at the Nankai Trough, southwest Japan, *J. Geophys. Res.*, 89, 3087-3101, 1984.
- Turcotte, D. L., and G. Schubert, *Geodynamics: Applications of Continuum Physics to Geological Problems*, 450 pp., John Wiley, New York, 1982.
- Von Tish, D. B., R. W. Allmendinger, and J. W. Sharp, History of Cenozoic extension in the central Sevier Desert, west-central Utah, from COCORP seismic reflection data, *Am. Assoc. Petrol. Geol. Bull.*, 69, 1077-1087, 1985.
- Webb, G. W., Stevens and earlier Miocene turbidite sands, San Joaquin Valley, California, in *Lake Miocene Geology and New Oil Fields of the Southern San Joaquin Valley*, AAPG-SEG-SEPM Pacific Section Guidebook, Am. Assoc. Pet. Geol., Tulsa, Okla., 1977.
- Whitehead, R.L., R.W. Harper, and H.G. Sisco, Hydrologic changes associated with the October 28, 1983, Idaho earthquake, *Pure Appl. Geophys.*, 122, 280-293, 1984.

G. C. P. King, U.S. Geological Survey, Box 25046, MS 966, Denver Federal Center, Denver, CO 80225.

J. B. Rundle, Division 5541, Sandia National Laboratories, Albuquerque, NM 87185.

R. S. Stein, U.S. Geological Survey, 345 Middlefield Road, MS 977, Menlo Park, CA 94025.

(Received December 21, 1987;
revised May 24, 1988;
accepted July 1, 1988.)